URSI GASS 2023, Sapporo, Japan, 19 – 26 August 2023

Traveling Ionospheric Disturbances detection: a TEC detrending techniques comparison and a study of their impact on extracted parameters

Marco Guerra*(1)(2), Claudio Cesaroni(2), Luca Spogli(2,3) and Mattia Crespi(1)
(1) Università "La Sapienza", Rome, Italy; e-mail: marco.guerra@ingv.it
(2) Istituto Nazionale di Geofisica e Vulcanologia, Rome, Italy
(3) SpacEarth Technology, Rome, Italy

Abstract

Thanks to the advances in the remote sensing of the Earth's Ionosphere through GNSS-derived Total Electron Content (TEC), we are now capable of detecting and characterizing wavy features in both post-processing and, to some extent, in real-time (RT). Therefore, this study aims at understanding and compare how different TEC detrending techniques and their settings impact the capabilities to extract wave parameters, such as amplitude and period. Moreover, the impact of general algorithm settings, like Ionospheric Piercing Point (IPP) height and elevation cut-off angle on the characterization capabilities is investigated. Finally, due to the growing interest in the RT detection and classification of Traveling Ionospheric Disturbances (TIDs), the study proposes and investigates possible techniques for the estimation of the TID amplitude in a near-RT (NRT) scenario.

1 Introduction

TIDs are plasma density fluctuations that propagate as waves through the ionosphere at a wide range of frequencies and velocities [1] and are usually classified according to those parameters into Small, Medium, and Large scale TIDs (SSTID, MSTID, and LSTID, respectively). Normally, TIDs are generated by the coupling of the neutral and ionized atmosphere [2], with gravity and acoustic neutral waves forcing a movement on ions due to collisions with neutral particles. Generally, LSTIDs are caused by geomagnetical activity [3] while MSTIDs can be related to natural hazards, (e.g. earthquakes, tsunamis, volcanic eruptions), neutral weather [2], and other phenomena related to the changes in the ionizing radiation from the Sun (e.g. solar terminator passages, solar eclipse, etc.)
In addition to being of scientific interest, TIDs are as well a driver for GNSS and HF degradation, especially at middle latitudes. TIDs can cause disturbances up to 20% of the background electron density, are responsible for an increase in cycle slip occurrence [4], and are a "Silent accuracy killer" [Ivan Galkin] as they are hardly detectable when affecting the GNSS signals received at the ground. This explains why it is utterly important to detect and characterize them in real-time, making it possible to develop mitigation techniques and forecasting algorithms. At the moment, there are only a few GNSS-based algorithms for the RT or NRT detection of TIDs; such as VARION [5] and GUARDIAN [6].
Now, given the importance of TID detection and characterization, follows that it is necessary to know the reliability of the techniques that are used to extract the wavy feature of interest from the TEC time series and to evaluate their impact on the extracted parameters.

2 Data and Methods

In order to create a representative database, we used 2 years' worth of data (2009, solar min, and 2014, solar max) gathered by a geodetic station belonging to the INGV's Rete Integrata Nazionale GNSS (RING), which is located close to Altamura, Apulia, Southern Italy. The data used were in the form of 30s RINEX files, and calibrated TEC was retrieved through the Ciraolo calibration technique [7].
To better compare different wave extraction techniques (some are detrending and some are filtering algorithms), we removed the high-frequency components performing a moving average. Now that the background arc (i.e. a continuous set of GNSS observations from a receiver-satellite pair) database is generated (about 15000 arcs), we need to add the wavy "synthetic" feature. To do so, we considered a 2D wave field that propagates at a given height (considered equal to the IPP height):

$$dTEC(x,y,t) = Asin(\frac{2\pi x}{\lambda}\cos\theta + \frac{2\pi y}{\lambda}\sin\theta + \frac{2\pi vt}{\lambda}) \quad (1)$$

Where A is the wave amplitude, λ is the wavelength, θ is the azimuth of propagation, and, lastly, v is the TID speed. Two different wave fields have been implemented, one representing an LSTID and one representing an MSTID. The two wave field parameters were set according to climatological values [1], [8] as shown in Table 1.
To extract wavy features from the TEC signal, 6 different detrending/filtering techniques have been applied to the wavy, smoothed arc:

1. Gaussian-weighted moving average
2. Multi-order numerical difference [1]
3. Third order Savitzky-Golay filter
4. 8th-order polynomial detrending
5. Finite Impulse response (FIR) bandpass filter
6. Fast Iterative Filtering (FIF) [9] bandpass filter

The techniques' main parameters were set according to the usual LSTIDs and MSTIDs ones, with the most impactful being the period. The period band considered for MSTIDs was between 5 and 30 minutes, while for LSTIDs the 40-90 minutes band was used.

Once the detrended database is successfully generated it was possible to investigate the amplitude and period error induced by the wave extraction technique. In particular, we defined the amplitude error (AE) as the difference between the given detrended arc and the wave field calculated at the IPP location. Regarding the period error instead, we used the normalized cross-correlation between the two signals to investigate how likely they are in the time domain.

Once the effect on the amplitude and period error introduced by the detrending algorithm is evaluated, the focus is moved to the effect on the wave period induced by the nature of the sensing instrument. Since our IPPs are moving across the TID, the measured wave will suffer a doppler effect, which is directly related to the elevation and height of the ionospheric shell. Thus, to investigate this phenomenon detrending techniques are not necessary, because the doppler effect depends only on the relative velocity between the IPP and the TID. Therefore, since the TID velocity vector is set, we hence need to derive the IPP velocity vector for each data sample. Once the relative velocity vector is evaluated, we can calculate the doppler effect thanks to the following equation:

$$f' = f(1 + \frac{v_{REL}}{v_{TID}}) \quad (2)$$

Where v_{REL} is the TID-IPP relative velocity, v_{TID} is the TID speed, f is the original wave frequency and f' is the detected frequency. Now, since the IPP velocity depends strongly on the satellite elevation and IPP height, we investigated as well the doppler induced error statistics for different values of the two parameters. This allows inferring the expected error given the ionospheric shell height and the elevation cut-off angle.

Lastly, we want to investigate how detrending different NRT available observables impacts the retrieved amplitude. VARION, for example, works by investigating the integrated Geometry-Free linear combination (GFLC) time difference, which is basically the uncalibrated (i.e. including the DCBs affecting TEC measurements) slant TEC (sTEC). Detrending such an observable (hereafter referred as VARION) will indeed induce an error in the wave amplitude proportional to the calibration bias times the mapping function. Despite that, such a technique has proven to be reliable in estimating the wave period [5]. Bearing this in mind, we proposed 2 NRT observables derived from the integrated GF time difference. The first one is simply the integrated GF multiplied times the mapping function (verticalization), while the second one is like the previous one but with an intermediate step, which is to estimate sTEC before verticalizing through NeQuick2 [10]. These latter 2 observables will be henceforth called vVARION and vNeVARION. All the 3 techniques presented are not computationally demanding and thus a good option for NRT operations. To quantify the AE we fixed a detrending technique and then considered as ground truth the detrended calibrated vTEC, which is confidently assumed to be the most reliable TEC estimate and thus normally used in post-processing studies.

3 Results

Figure 1 reports the AE statistic. FIF is found to perform better than the other techniques in terms of AE. Since our distributions are highly non-normal, we looked at the median together with percentiles rather than at the mean and standard deviation. Figure 1 also shows, how the median AE value for all techniques is close to 0, with FIF showing the smallest one for MSTIDs and the second smallest for LSTIDs. Moreover, FIF shows as well the smallest 16-84 percentile in both TID scenarios and the best/second best 2.5-97.5 percentile for LSITD/MSTID, respectively.

Now, from Figure 2 we can investigate the ability of the different techniques at preserving the decomposed signal in the time domain, which is necessary when using interferometry techniques for speed/azimuth retrieval. Focusing on the MSTID case, the multi-order numerical difference has both the smallest mean and standard deviation, with FIF being respectively the second and third best. Instead, looking at LSTID statistics, FIF shows both the smallest average and standard deviation of the correlation error. Considering everything discussed above, we can confidently affirm that FIF is the best detrending technique overall for both TID scenarios since it ranks among the best techniques in both errors for both TIDs.

Now that the results for the wavy feature extraction comparison have been shown, the focus is moved instead to the effects of general settings on the extracted parameters. Figure 3 shows the cumulative distribution function of the percentage period error induced by the IPP movement as a function of 2 different ionospheric shell heights and 5 different elevation cut-offs. Looking at the different distributions, it is easily noticeable how higher shell height and lower cut-offs correspond to higher errors on average. This is easily explainable by the direct geometrical relationship between the IPP velocity and both the shell height and the elevation. Moreover, Figure 3 shows as well how slower TIDs are more prone to the doppler effect since the TID to IPP speed ratio is smaller. To quantify this, let's look at the value of the period error for P(x)=0.8 for the MSTID scenario. Considering a shell height of 250 km, the 0.8 value for 20° and 60° elevation cut-offs are respectively 23 % and 37 %. Instead, setting the IPP height to 350 km, the values are respectively 33 % and 53 %. Here, we stress that those values are a function of both the TID speed/azimuth and the GNSS station's geographic location. Nevertheless, having used climatological values for TID speed and azimuth, the values are assumed to still be representative of what a mid-latitude-based user might expect.

To conclude, Figure 4 investigates the AE for different observables that might be used in an NRT scenario. Specifically, Figure 4 shows the median together with the 16-84 and 2.5-97.5 percentiles for the 3 different

techniques. From the different statistical values, we can confidently affirm that the verticalized bias-corrected VARION output (vNeVARION) is the one that most accurately resembles the output of the detrend calibrated vTEC. Looking at numerical values for the vNeVARION, the 2.5/97.5 percentile values are respectively -18/18 and -27.6/27.8 mTECu for LSTID and MSTID, which is indeed a really good degree of accordance.

4 Discussion and Conclusions

In this section, we discuss the significance of our results in terms of assessing how the assumption made might affect the likelihood of our synthetic data to real data. First, we assumed the TID to be localized only in a thin-shell ionospheric layer, which should be reliable since vTEC is an integrated quantity and most of the ionospheric plasma is located close to the peak density height. Moreover, to make our database more representative, we considered 2 whole years of data, which should cover all possible observational geometry and different ionospheric background conditions. Finally, since the GNSS receiver considered in this study is located in the European sector at mid-latitude, the statistical values obtained in this study might not be representative of high- and low-latitude regions, but the general picture and hence the rank of the technique should still be the same.

To conclude, thanks to the statistical analysis performed we had the possibility to quantitatively rank different detrending techniques in terms of extracted parameters, with the novel FIF-based bandpass filter showing the best overall stats. Furthermore, we were able to quantify the period error induced by the IPP movement, which could be useful in avoiding setting blindly the elevation cut-off angle, but rather basing it on the maximum acceptable percentage error given the kind of TID of interest. Finally, the investigation of the AE for the different considered detrended NRT observables showed how vNeVARION shows very good accordance with detrended calibrated data, which is indeed an encouraging result for NRT provided also its computational features.

5 Tables and Figures

5.1 Tables

Table 1. MSTID and LSTID parameters used to generate the wavefield described in Equation 1.

	MSTID	LSTID
Amplitude (A) [TECu]	0.2	0.4
Wavelength (λ) [km]	1800	200
Azimuth (θ) [°]	150	195
Speed (v) [m/s]	200	400
Period [min]	16.7	75

5.2 Figures

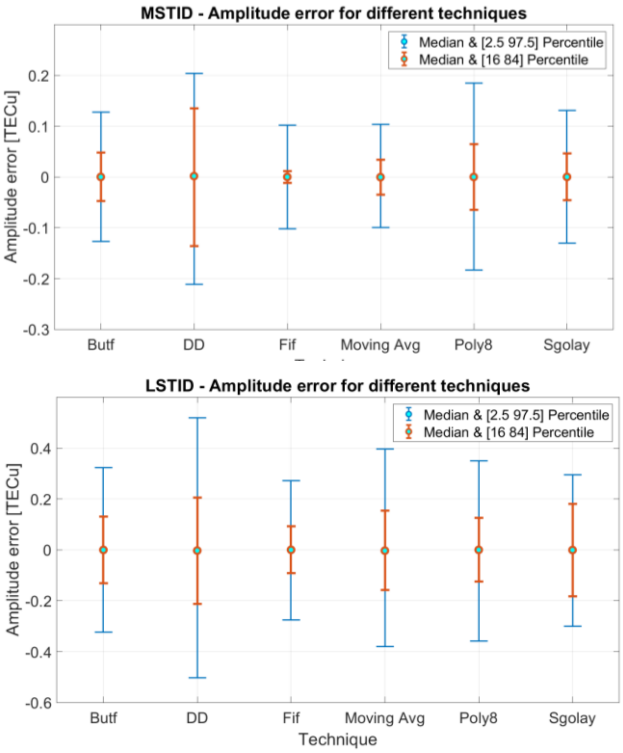

Figure 1. Median and 16/84 and 2.5/97.5 percentiles values for different detrending techniques for both MSTID and LSTID. Butf and DD represent respectively the bandpass filter and the multi-order numerical difference. The database was generated with IPP height and elevation cut-off set to 350km and 20° respectively.

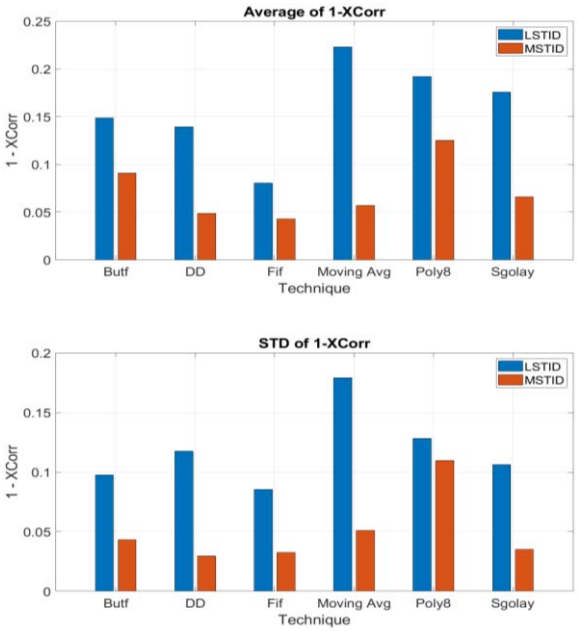

Figure 2. Average (top) and standard deviation (bottom) of the correlation error for the 6 different techniques. The database was the same as in Figure 1.

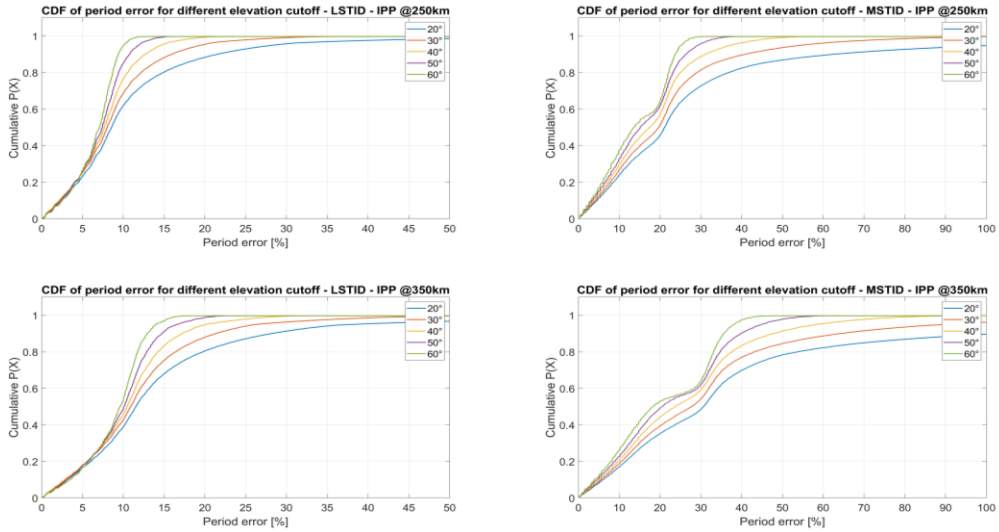

Figure 3. Cumulative distribution function plots of percentage period error for 350 (bottom) and 250 km (top) of IPP height and for both MSTID (right) and LSTID (left). Differently colored lines correspond to different elevation cut-off values.

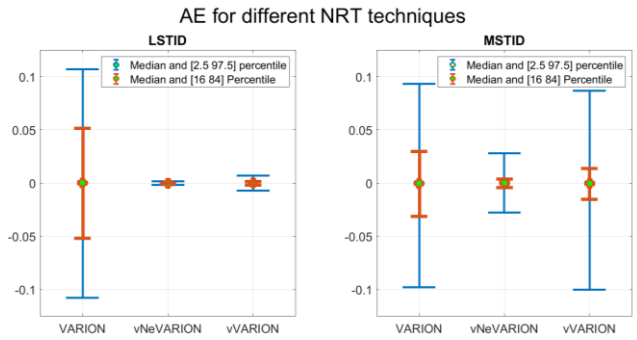

Figure 4. Median and percentiles of amplitude error for different detrended NRT observables with respect to calibrated detrended vTEC for both MSTID (right) and LSTID (left). The dataset was the same as in Figure 1.

Acknowledgments

The authors wish to gratefully thank the Telecommunications/ICT for Development (T/ICT4D) Laboratory of the Abdus Salam International Centre for Theoretical Physics and B. Nava for the NeQuick2 model. We would like to thank as well G. Savastano and M. Ravanelli for sharing the VARION code and A. Cicone for the FIF algorithm.

References

[1] M. Hernández-Pajares, J. M. Juan, and J. Sanz, 'Medium-scale traveling ionospheric disturbances affecting GPS measurements: Spatial and temporal analysis', *J. Geophys. Res. Space Phys.*, vol. 111, no. 7, Jul. 2006, doi: 10.1029/2005JA011474.

[2] E. Astafyeva, 'Ionospheric Detection of Natural Hazards', *Rev. Geophys.*, vol. 57, no. 4, pp. 1265–1288, Dec. 2019, doi: 10.1029/2019RG000668.

[3] C. Cesaroni *et al.*, 'The First Use of Coordinated Ionospheric Radio and Optical Observations Over Italy: Convergence of High-and Low-Latitude Storm-Induced Effects', *J. Geophys. Res. Space Phys.*, vol. 122, no. 11, p. 11,794-11,806, Nov. 2017, doi: 10.1002/2017JA024325.

[4] M. Poniatowski and G. Nykiel, 'Degradation of kinematic ppp of gnss stations in central europe caused by medium-scale traveling ionospheric disturbances during the st. Patrick's day 2015 geomagnetic storm', *Remote Sens.*, vol. 12, no. 21, pp. 1–15, Nov. 2020, doi: 10.3390/rs12213582.

[5] G. Savastano *et al.*, 'Real-time detection of tsunami ionospheric disturbances with a stand-alone GNSS receiver: A preliminary feasibility demonstration', *Sci. Rep.*, vol. 7, 2017, doi: 10.1038/srep46607.

[6] L. Martire *et al.*, 'The GUARDIAN system-a GNSS upper atmospheric real-time disaster information and alert network', vol. 27, p. 32, 2023, doi: 10.1007/s10291-022-01365-6.

[7] L. Ciraolo, F. Azpilicueta, C. Brunini, A. Meza, and S. M. Radicella, 'Calibration errors on experimental slant total electron content (TEC) determined with GPS', *J. Geod.*, vol. 81, no. 2, pp. 111–120, Feb. 2007, doi: 10.1007/s00190-006-0093-1.

[8] E. Blanch, A. Segarra, D. Altadill, V. Paznukhov, and J. M. Juan, 'Large Scale TIDs climatology over Europe using HF Interferometry method'.

[9] A. Cicone and H. Zhou, 'Numerical analysis for iterative filtering with new efficient implementations based on FFT', *Numer. Math.*, vol. 147, no. 1, pp. 1–28, Jan. 2021, doi: 10.1007/s00211-020-01165-5.

[10] B. Nava, P. Coisson, and S. M. Radicella, 'A new version of the NeQuick ionosphere electron density model', *J. Atmospheric Sol.-Terr. Phys.*, vol. 70, no. 15, pp. 1856–1862, 2008, doi: 10.1016/j.jastp.2008.01.015.